Dalton Transactions

PERSPECTIVE

View Article Online
View Journal | View Issue

Cite this: *Dalton Trans.*, 2017, **46**, 6146

Templated and template-free fabrication strategies for zero-dimensional hollow MOF superstructures

Hyehyun Kim and Myoung Soo Lah *

Received 1st February 2017,
Accepted 14th March 2017

DOI: 10.1039/c7dt00389g

rsc.li/dalton

Various fabrication strategies for hollow metal–organic framework (MOF) superstructures are reviewed and classified using various types of external templates and their properties. Hollow MOF superstructures have also been prepared without external templates, wherein unstable intermediates obtained during reactions convert to the final hollow MOF superstructures. Many hollow MOF superstructures have been fabricated using hard templates. After the core–shell core@MOF structure was prepared using a hard template, the core was selectively etched to generate a hollow MOF superstructure. Another approach for generating hollow superstructures is to use a solid reactant as a sacrificial template; this method requires no additional etching process. Soft templates such as discontinuous liquid/emulsion droplets and gas bubbles in a continuous soft phase have also been employed to prepare hollow MOF superstructures.

1. Introduction

During the last several decades, metal–organic frameworks (MOFs), assembled by metal ions (or metal clusters) and organic ligands through coordination bonds, have received tremendous attention as a new class of porous crystalline materials. The diversity and tunability of microporous MOFs have prompted investigations into their potential applications in various areas such as gas storage/capture and separation, catalysis, drug delivery, and sensing.[1] Superstructures of such objects, known as higher-order meso/macroscopic structures, have also received considerable attention because of their collective and/or synergistic effects originating from the assemblies in addition to the inherent functionality of the object itself.[2] More recently, many researchers have endeavored to prepare MOF superstructures such as zero-dimensional (0-D) hollow spheres, one-dimensional (1-D) fibers, two-dimensional (2-D) films, and hierarchically extended three-dimensional (3-D) structures on the meso- and macroscopic scales.[3]

Department of Chemistry, UNIST, Ulsan 44919, Korea. E-mail: mslah@unist.ac.kr

Hyehyun Kim

Hyehyun Kim received her bachelor's degree in chemistry from Hanyang University, Korea, in 2012. She is doing her PhD degree at the Department of Chemistry, Ulsan National Institute of Science and Technology under the supervision of Prof. Myoung Soo Lah. She is currently working on the preparation of new MOFs based on zirconium and the modification of their pore environments and studying their various properties including gas sorption behaviors and catalytic properties.

Myoung Soo Lah

Myoung Soo Lah attended Seoul National University, Korea, for his BSc and MSc and earned his PhD in chemistry from the University of Michigan, Ann Arbor, in 1991. After his post-doctoral research in macromolecular crystallography from the same university, he became a faculty member of the department of chemistry, Hanyang University in 1992 and then moved to Ulsan National Institute of Science and Technology in 2010, where he is presently a professor of the department of chemistry. He is interested in the development of metal–organic systems such as MOPs and MOFs for application in the areas of storage, capture/separation, and catalysis.

Here, we focus on fabrication strategies for 0-D hollow MOF superstructures. (Hereafter, we will simply refer to them as "hollow".) These strategies are closely related to those for hollow metal (M)/metal oxide (MO) superstructures. Many hollow M/MO superstructures have been reported *via* various fabrication strategies.[4] Hollow MO nanostructures have been obtained *via* the Ostwald ripening process without templates.[5] During the recrystallization of crystallites, mass transfer from smaller crystallites in the core region to larger crystallites in the shell region of a crystallite aggregate intermediate led to a hollow superstructure without relying on an external template. The most typical approach for hollow superstructures is to prepare a core–shell intermediate using a hard solid template and subsequently removing the hard solid template from the core–shell structure.[6] The other approach for forming hollow superstructures is to use a solid reactant itself as a sacrificial template.[7] A hollow nanocrystal can be synthesized using a solid reactant as a sacrificial template through the Kirkendall effect, wherein the hollow cavity forms near the interface between two reactants, namely a solid sacrificial template and another incoming reactant, due to different interdiffusion rates of the two reactants.[8a,b] Hollow nanocrystals of cobalt oxide/chalcogenides were formed by the reaction of cobalt nanocrystals as a sacrificial template with oxygen/chalcogens, which was attributed to the dominant outward diffusion of the sacrificial cobalt nanocrystals, thus generating a single cavity in the center of the metal oxide/chalcogenide nanoparticles.[8c] Hollow superstructures can also be obtained at the interface between discontinuous emulsion droplets/supramolecular micelles and a continuous fluid phase using liquid droplets/micelles as a soft template.[9]

Here, we review strategies to prepare hollow MOF superstructures. Similar to the fabrication strategies for hollow M/MO superstructures, they are classified based on the presence or absence of an external template and the types and properties of the templates (Scheme 1). The advantages and disadvantages of these strategies are also discussed (Table 1).

2. Template-free strategies

2.1. Ostwald ripening

Like hollow MO nanostructures, hollow MOF superstructures can be obtained by a one-pot solvothermal reaction *via* the Ostwald ripening mechanism without a template. The solvothermal reaction of $FeCl_3{\cdot}6H_2O$ with 1,1′-ferrocenedicarboxylic acid (H_2FcDC) in *N*,*N*-dimethyl formamide (DMF) produced hollow spherical particles with microporous coordination polymer shells.[10a] The hollow spherical superstructure was generated by recrystallization *via* mass transfer from the core region with smaller crystallites to the shell region with larger crystallites in the organized crystallite aggregate intermediate (Fig. 1). The reaction temperature, reaction time, and molar ratio of the reactants played important roles in tuning the cavity dimensions of the hollow MOF microsphere. The preparations of several other hollow MOF microspheres were also reported *via* the same Ostwald ripening mechanism.[10b–d] In addition to the above-mentioned reaction conditions, *i.e.* the reaction temperature, reaction time, and molar ratio of the reactants, the concentrations of the reactants and the solvents used also played important roles in the formation of crystallite aggregates as kinetic intermediates and the subsequent thermodynamic ripening to hollow MOF microstructures. Ostwald ripening is very convenient for the formation of hollow MOF superstructures since it does not require an external template. However, there have been no systematic investigations to discover the appropriate reaction conditions for the formation of crystallite aggregates as kinetic intermediates and for the subsequent thermodynamic ripening to form hollow superstructures.

2.2. Surface-energy-driven mechanism

In 2014, Wang *et al.* demonstrated the one-pot preparation of hollow superstructures *via* another template-free mechanism, a surface-energy-driven mechanism.[11a] The solvothermal reaction of benzenedicarboxylic acid (H_2BDC) with a mixture of Zn^{2+} and Fe^{3+} ions in a mixed *N*,*N*-dimethylacetamide (DMA)/ethanol solvent in the presence of poly(vinylpyrrolidone) (PVP) as a stabilizing reagent produced an amorphous infinite coordination polymer (ICP) with a well-defined hollow octahedral morphology (labeled as Fe^{III}-ICP). They concluded that a surface-energy-driven mechanism was responsible for the formation of hollow octahedral nanocages because they observed that during the initial stage of the reaction, concave octahedra with high surface energies formed. These concave octahedra subsequently transformed into hollow octahedra with lower surface energies *via* an inside-out mass transfer process (Fig. 2a and b).

Xun Wang's group reported other hollow superstructures, namely hollow nanocubes assembled from a 3-D MOF (*i.e.*, MOF-5) and hollow nanocubes assembled using a 2-D MOF sheet (*i.e.*, MOF-2), *via* the same surface-energy-driven mechanism.[11b] First, kinetic intermediates were quenched during the solvothermal reaction of H_2BDC with Zn^{2+} and Ni^{2+} ions in a DMA/EtOH mixed solvent. These intermediates were then dispersed in different volumes of EtOH and for different lengths of time, thereby forming 3-D mesoporous nanocubes, concave nanocubes with hollow interiors, and nanocubes with a cavity in the center *via* the surface-energy-driven mechanism. All of these nanostructures have the same MOF-5 crystal lattice

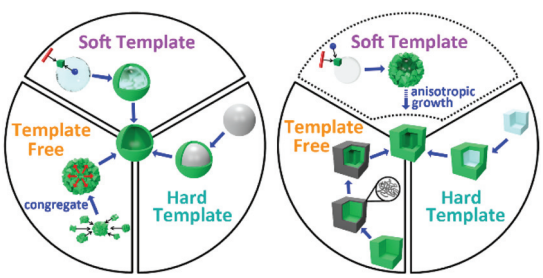

Scheme 1 Fabrication strategies for hollow MOF superstructures.

Table 1 Comparisons of the features and the advantages and disadvantages of various strategies for hollow MOF superstructures

Strategies		Types		Features	Advantages	Disadvantages
Template free		Ostwald ripening Self-template mechanism Surface-energy-driven mechanism		- Polycrystalline aggregates - Spherical morphology - Non-spherical morphology	- No external template - No etching process	- Difficulty in finding the proper conditions for kinetic intermediates
		Surface-protected selective etching strategy		- Single-crystalline hollow structure	- Facile control of the morphology of the hollow structure	- Deterioration of the hollow structure during the etching process
		Quenched core–shell intermediate		- Controlled non-spherical morphology		- Need to prepare epitaxially grown core–shell structures with selective core etching possibility
Template	Hard	Amorphous solid template		- Polycrystalline aggregates - Spherical morphology	- Facile synthesis of the amorphous solid template - Diverse template surface modifications - Easily etched	- Limited to spherical morphology - Deterioration of the hollow structure during the etching process
		Crystalline solid template		- Single-crystalline template - Controlled non-spherical morphology	- Facile control of the morphology and dimensions of the hollow structure	- Need to prepare epitaxially grown core–shell structures with selective core etching possibility
		Core–shell template		- Polycrystalline aggregates - Yolk–shell hollow structure	- No need for an etching process	- No morphology control
		Sacrificial template	Sacrificial core–shell template	- Polycrystalline aggregates - Sacrificial shell of the core–shell template - Yolk–shell hollow structure	- No need for an etching process	- No morphology control
			Sacrificial single-crystal template	- Controlled non-spherical morphology	- No need for an etching process - Facile control of the morphology and dimensions of the hollow structure	- Need to find proper conditions for sacrificial templating
	Soft	Micelle template		- Polycrystalline aggregates - Spherical morphology	- Facile encapsulation of the guest materials	- Need to find the proper removal process for the micelle template
		Cell-wall template		- Polycrystalline aggregates - Controlled non-spherical morphology - Composite of the MOF and cell wall	- No need for a template removal process - Facile encapsulation of the guest materials	- Limited to mild synthetic conditions
		Liquid template Spray drying strategy Gas template		- Polycrystalline aggregates - Spherical morphology - Polycrystalline aggregates - Both spherical and non-spherical morphologies	- Facile template removal	- Limited to spherical morphologies - Need to find proper conditions for non-spherical morphologies

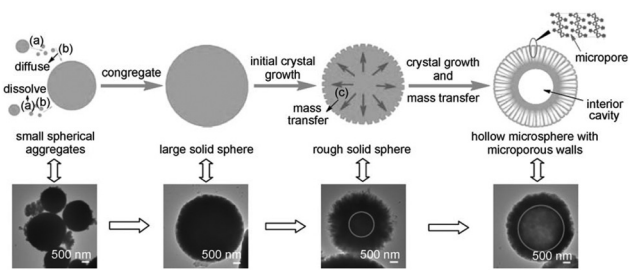

Fig. 1 Proposed formation process for iron-based ferrocenyl coordination polymer microspheres *via* the Ostwald ripening mechanism and the corresponding TEM images. Reprinted with permission from ref. 10*a*. © 2010 Wiley-VCH.

with the same molar ratio of Zn to Ni. In contrast, the unquenched reaction under the same reaction conditions produced hollow nanocubes assembled using a 2-D MOF-sheet. The investigation into the evolution of the hollow nanocubes revealed the sequential formations of uniform Zn/Ni-MOF-5 cubic nanoparticles, concave Zn/Ni-MOF-5 nanocubes covered with 2-D Zn/Ni-MOF-2 sheets, and hollow nanocubes composed of 2-D Zn/Ni-MOF-2 sheets (Fig. 2c). First, Zn/Ni-MOF-5 nanocubes rapidly form as kinetic intermediates due to high concentrations of metal ions and organic ligands in the initial stage of the reaction. Then, the Zn/Ni-MOF-5 dissolves in the core region of the nanocubes, and the 2-D Zn/Ni-MOF-2 sheets crystallize in the shell region of the nanocubes. Finally, hollow nanocubes made of thermodynamically favorable Zn/Ni-MOF-2

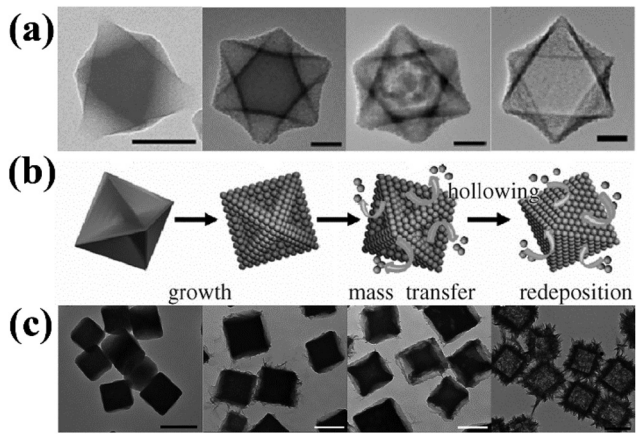

Fig. 2 (a) TEM images of Fe^{III}-ICP collected at different reaction times and (b) the proposed schematic diagrams of the corresponding structures during the formation process. Scale bars: 100 nm. Reproduced with permission from ref. 11*a*. © 2014, Wiley-VCH. (c) TEM images of the evolution from Zn/Ni-MOF-5 to Zn/Ni-MOF-2 hollow nanocubes assembled from nanosheets after different reaction times. Scale bars: 500 nm. Reproduced with permission from ref. 11*b*. © 2014 Wiley-VCH.

nanosheets are formed using the pre-formed Zn/Ni-MOF-5 nanocubes as a sacrificial template.

2.3. Self-template mechanism

In 2015, Oh *et al.* reported the one-pot synthesis of hollow MOF superstructures using Zn^{2+} ions and 1,3,5-benzenetricarboxylic acid (H_3BTC) *via* a solvothermal reaction in DMF with no external template.[12] The authors proposed a self-templated multi-stage mechanism consisting of (1) the formation of spherical solid microparticles as self-templates during the first stage of the reaction, (2) subsequent simultaneous dual processes consisting of new crystalline MOF particle growth on the surface of the spherical solid microparticle and the spontaneous dissolution of the spherical solid microparticle, and (3) the final formation of hollow microporous MOF microparticles as a thermodynamic product (Fig. 3). However, the possible conditions for the formation of the self-templates as kinetic intermediates and the reason for the subsequent crystalline MOF particle growth on the surface of the self-template were not discussed.

Template-free strategies are much more convenient than the other strategies since they are usually a one-pot process and do not require additional etching process. However, it remains challenging to find the appropriate conditions for unstable intermediates such as organized crystallite aggregates, concave octahedra with high surface energy, and self-templates. In addition, the transformation mechanisms from the unstable kinetic intermediates to the stable thermodynamic hollow superstructures are not well understood.

2.4. Surface-protected selective etching strategy

In 2012, Yamauchi *et al.* showed the stepwise preparation of hollow cubic Fe Prussian blue (Fe-PB) nanoparticles[13*a*] and

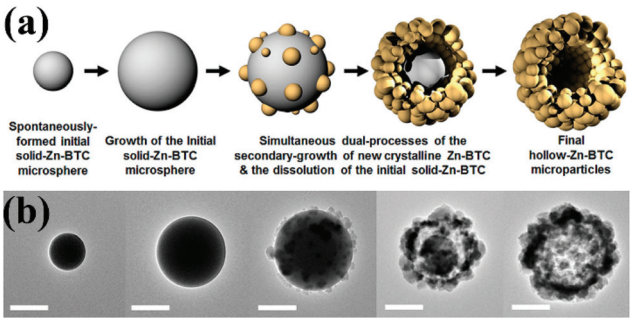

Fig. 3 (a) Schematic representation of the production of hollow-Zn-BTC microparticles *via* a self-templated formation mechanism and (b) TEM images of the corresponding schematic diagrams. Scale bars: 1 μm. Reproduced with permission from ref. 12. © 2015 American Chemical Society.

their CoFe-PB and MnFe-PB analogues[13*b*] with crystalline microporous shells using the corresponding surface-protected mesocrystals (*i.e.*, oriented aggregates of PB nanocrystals) as precursors. The hollow superstructures were formed in a HCl solution by selectively etching the core region of the cubic PB mesocrystals with their surfaces protected by PVP (Fig. 4). Lin, Pang and Eddaoudi's research team also reported the stepwise preparation of cubic hollow Ga-**soc**-MOF superstructures using the same surface-protected selective etching strategy.[13*c*] The hollow MOF nanostructures were obtained *via* the controlled etching of the core region of the surface-protected Ga-**soc**-MOF cubes using HCl solution as the etching agent.

Recently, Caruso *et al.* prepared hollow MOF nanostructures using phenolic acids, such as tannic acid (TA) and gallic acid (GA), both as protecting and etching reagents.[13*d*] The hollow superstructures were obtained by incubating preformed crystals of the MOF, ZIF-8 polyhedra or MIL-68 rods, in the phenolic acids for several minutes. While the surface region of the MOF was protected by the formation of metal–phenolate networks, the free protons released from the phenolic acids dissolved the inner part of the MOF framework. The shape and dimensions of the non-hollow structures were maintained after the etching process, and thus, the shape and dimensions of the hollow superstructures fabricated *via* the surface-protected selective etching strategy could be controlled by the preparation of the initial non-hollow structures.

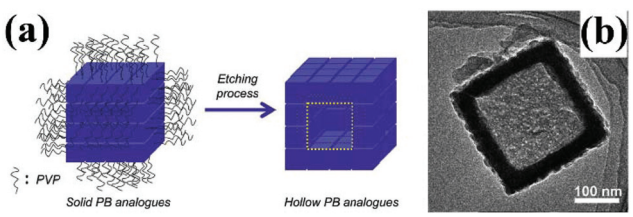

Fig. 4 (a) Schematic illustration of the synthesis of hollow MFe-PB analogue nanocubes by chemical etching with PVP as a protecting agent. (b) A TEM image of an analogous hollow CoFe-PB nanocube. Reproduced with permission from ref. 13*b*. © 2012 Wiley-VCH.

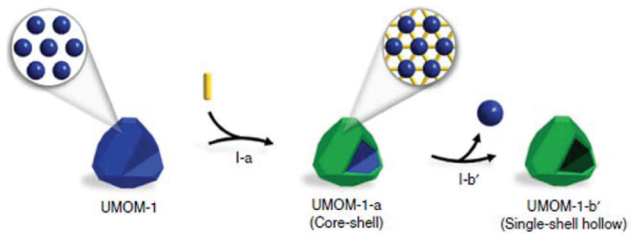

Fig. 5 Schematic representation of a hollow UMOM-1-b′ superstructure *via* a quenched core–shell intermediate. Reproduced with permission from ref. 14. © The Author(s) 2017.

2.5. Quenched core–shell intermediate

In 2017, Kwak and Choe's research team reported hollow MOF superstructures fabricated by selectively etching the metal–organic polyhedron (MOP) cores of MOP@MOF core–shell structures prepared as a precursor (Fig. 5).[14] The MOP@MOF core–shell precursor was obtained as a quenched intermediate during the single-crystal-to-single-crystal MOP-to-MOF conversion that occurs by inserting ditopic 1,4-diazabicyclo[2.2.2] octane (dabco) linkers into an MOP single crystal made of $[Cu_{24}(hip)_{24}]$ (H_2hip = 5-hydroxyisophthalic acid) building blocks in a cubic close-packed arrangement. The MOP-to-MOF transformation occurred from the surface to the core of the MOP crystals. If this transformation was quenched before it was completed, MOP@MOF core–shell structures could be obtained as an intermediate.

The surface-protected selective etching strategy and the quenched core–shell intermediate strategy are also template-free strategies. However, their processes are completely different from those of the other template-free strategies because they are multi-step processes. In both cases, after the "core–shell-like" or MOP@MOF core–shell structures are prepared as intermediates, the core regions of the core–shell structures were selectively etched to form the corresponding hollow MOF superstructures. Specifically, in the surface-protected selective etching strategy, the surfaces of the precursor MOFs were protected using a surface-protecting agent to form "core–shell-like" structures, and the unprotected core regions of the MOF were then selectively etched away. In the quenched core–shell intermediate strategy, the MOP cores of the MOP@MOF core–shell structures were selectively etched.

3. Hard template strategies

3.1. Amorphous solid template

The amorphous solid template strategy utilizes amorphous spherical particles as a hard solid template. Core–shell structures are obtained using spherical solid particles with a modified surface that can direct the efficient growth of the MOF shell on the surface. Hollow MOF superstructures can then be obtained by immersing the core–shell structures in an organic solvent that can selectively etch away the amorphous core.

In 2012, Oh *et al.* reported the preparation of a hollow MOF superstructure using a spherical polymer particle as an amorphous solid template.[15a] They prepared polystyrene (PS)@ZIF-8 core–shell structures by adding carboxylate-terminated PS spheres to a methanol solution containing 2-methylimidazole (2-MeIM) and $Zn(NO_3)_2$. Hollow ZIF-8 microspheres were induced by soaking the as-prepared PS@ZIF-8 core–shell microspheres in DMF, which selectively dissolve the PS core (Fig. 6).

Other hollow MOF superstructures such as hollow MIL-100 (Fe) and hollow Cu-BTC (HKUST-1) nanospheres have been reported *via* the same amorphous solid template strategy.[15b] Each hollow MOF superstructure was prepared under the same reaction conditions for the corresponding pristine non-hollow MOF structure using sulfonate-terminated PS spheres as a spherical solid template instead of carboxylate-terminated PS spheres. The MOF shell thickness of the hollow MOF superstructures was controlled by repeating the MOF growth cycle on the PS@MOF core–shell microspheres.

3.2. Crystalline solid template

One of the advantages of the hard template strategy is that the morphology of the template can easily be controlled, thus enabling control of the size and shape of the hollow superstructure. However, controlling the shape *via* the amorphous solid template strategy is usually limited to spherical superstructures due to the inherent difficulties in fabricating non-spherical amorphous solid particles. However, non-spherical particles have been achieved *via* the crystalline solid template approach.

Talham *et al.* prepared core–shell nanocubes with the RbMnFe-PB core as a cubic crystalline solid template and the isostructural analogue RbMFe-PB (M = Co, Ni) as a shell (Fig. 7).[16a] The RbMnFe-PB core was selectively dissolved under mild conditions (namely, holding the core–shell nano-

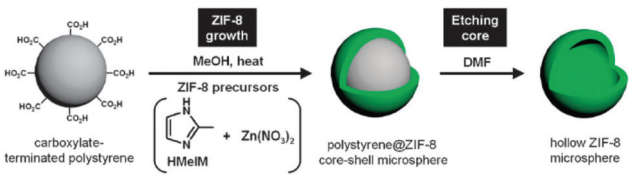

Fig. 6 Schematic diagram of the preparation of hollow ZIF-8 microspheres. Reprinted with permission from ref. 15a. © 2012 The Royal Society of Chemistry.

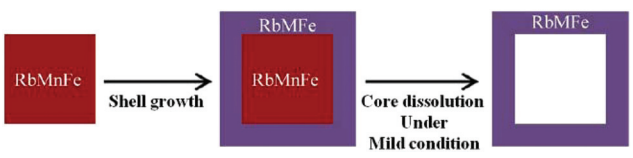

Fig. 7 Synthetic strategy for well-preserved hollow RbMFe (M = Co, Ni) nanocubes. Reproduced with permission from ref. 16a. © 2012 American Chemical Society.

cubes in water at 45 °C for 45 min) by exploiting its higher solubility relative to those of the other PB analogues, which resulted in well-preserved crystalline hollow nanocubes. The advantage of the crystalline solid template approach is that core–shell MOF nanostructures can be prepared *via* the epitaxial growth of an isostructural MOF shell on the crystalline template with no surface modification. The size- and shape-controlled hollow MOF superstructures can be obtained by selectively dissolving the unstable MOF core. Li and Wang's research team reported hollow MOF cubes and yolk–shell MOF cubes fabricated using epitaxially grown Fe-PB@NiFe-PB core–shell and NiFe-PB@Fe-PB@NiFe-PB double core–shell structures, respectively, *via* a stepwise selective etching process.[16b] After converting the Fe-PB part of the core–shell/double core–shell composites to $Fe(OH)_3$ in an alkaline solution, the $Fe(OH)_3$ region was selectively removed by washing with a HCl solution to obtain the hollow superstructures.

Wu and Li's research team prepared ZIF-67@ZIF-8 core–shell structures using Co(II)-based ZIF-67 with a rhombic dodecahedral morphology as a crystalline MOF template and isostructural Zn(II)-based ZIF-8 as a MOF shell.[16c] A subsequent solvothermal treatment of the resulting core–shell structure suspension in a methanol solution resulted in hollow ZIF-8 rhombic dodecahedral superstructures containing some interlaced flake-shaped Co-ZIF in the hollow cavity.

Muhler and Fischer's research team employed a modified two-step procedure to obtain the same hollow superstructure obtained by Wu and Li's research team.[16d] The solvothermal treatment of Co(II)-based ZIF-67 seed crystals dispersed in methanol with Zn^{2+} ions and 2-MeIM produced similar hollow ZIF-8 rhombic dodecahedral superstructures containing some interlaced flake-shaped Co-ZIF in the hollow cavity. The rhombic dodecahedral morphology of the hollow superstructures indicates that the seed crystals served as a crystalline hard template. However, the color change of the mother liquor from colorless to pinkish, which indicated the presence of Co^{2+} ions in solution, suggested the simultaneous partial etching of the ZIF-67 template during the formation of the hollow superstructures.

In 2015, Kuo and Tsung's research team prepared hollow ZIF-8 microcrystals by overgrowing a ZIF-8 shell in a methanol solution on a ZIF-8 core with water adsorbed in its pores (Fig. 8).[17] The water-permeated ZIF-8 cubes were re-suspended in methanol and then mixed with a 2-MeIM methanol solution. After adding $Zn(NO_3)_2$ dissolved in methanol into the solution containing the ZIF-8 cubes and 2-MeIM, the reaction solution was left undisturbed to produce hollow ZIF-8 superstructures. The ZIF-8 core dissolved to form a hollow cavity because of the change in the solution pH, which decreased due to the deprotonation of the 2-MeIM during the formation of the ZIF-8 shell. Since the ZIF-8 crystal cores in acidic aqueous conditions were less stable than the ZIF-8 crystal shells in acidic methanolic conditions, the core region of the ZIF-8 crystal was selectively dissolved. The powder X-ray diffraction (PXRD) pattern and N_2 sorption isotherms of the hollow MOF superstructures indicated that the hollow shells were

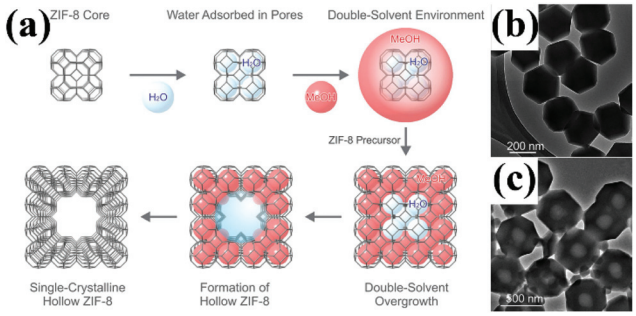

Fig. 8 (a) Schematic diagram of the preparation of a hollow ZIF-8 superstructure *via* double-solvent-mediated overgrowth. TEM images of (b) solid ZIF-8 crystals and (c) hollow ZIF-8 superstructures. Reproduced with permission from ref. 17. © 2015 The Royal Society of Chemistry.

crystalline and microporous. The hollow ZIF-8 superstructure could also be prepared by overgrowing the ZIF-8 shell in methanol solution on a ZIF-67 core instead of a ZIF-8 core. The energy-dispersive X-ray (EDX) mapping of the hollow ZIF-8 superstructures prepared using the ZIF-67 cubes as the core indicated that the Co^{2+} ions from ZIF-67 were mainly deposited on the inner surface of the hollow cavity. The deposition of the Co^{2+} ions in the hollow cavity suggested that the organic linkers from ZIF-67 were also entrapped in the same cavity.

The hollow MOF superstructures obtained *via* the crystalline solid template exhibited well-developed morphologies, which could be replicated from their parental crystalline templates. In addition, the shells of the hollow superstructures were crystalline and microporous when the template cores had been etched under mild conditions. However, this strategy was only applied to epitaxially grown core–shell structures made of isostructural MOFs with different stabilities.

3.3. Core–shell template

Tsung *et al.* reported the preparation of yolk–shell nanocrystal@ZIF-8 nanostructures using the Cu_2O shell of nanocrystal@Cu_2O core–shell nanostructures as a core–shell template (Fig. 9).[18] The addition of pre-prepared Pd@Cu_2O

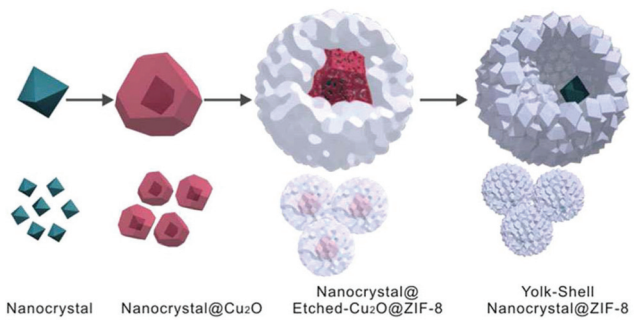

Fig. 9 Growth procedure for Pd@ZIF-8 yolk–shell nanostructures using a Pd@Cu_2O core–shell structure as a core–shell template. Reprinted with permission from ref. 18. © 2012 American Chemical Society.

core–shell dispersed in a $Zn(NO_3)_2$ methanol solution into a 2-MeIM methanol solution generated yolk–shell Pd@ZIF-8 nanostructures. The polycrystalline ZIF-8 layer spontaneously formed on the core–shell template, while the Cu_2O shell was etched away from the core–shell template. These two processes occurred simultaneously because the deprotonation of 2-MeIM during the formation of ZIF-8 changed the pH of the reaction medium to mildly acidic, thus leading to the oxidative dissolution of the Cu_2O shell. However, although the Pd@Cu_2O core–shell nanostructures have good morphologies with well-developed surfaces, the ZIF-8 shells of the yolk–shell Pd@ZIF-8 nanostructures were assembled aggregates of polycrystalline ZIF-8 nanocrystals.

3.4. Sacrificial template strategies

A sacrificial template simultaneously serves as both a template and reactant during the formation of a hollow superstructure. The sacrificial template strategy does not require an additional etching process since the template is consumed during the reaction.

3.4.1. Sacrificial core–shell template. Huo *et al.* prepared yolk–shell nanoparticle (NP)@MOF heterosuperstructures using the MO shell of NP@MO core–shell nanostructures as a sacrificial core–shell template (Fig. 10).[19] This strategy is very similar to that employed by the Tsung group to prepare yolk–shell Pd@ZIF-8 nanostructures.[18] The solvothermal reaction of the H_3BTC solution in a benzyl alcohol/ethanol mixed solvent after the addition of dispersed NP@Cu_2O core–shell nanostructures in benzyl alcohol led to yolk–shell NP@HKUST-1 heterosuperstructures because only the shells of the NP@Cu_2O core–shell nanostructures were consumed during the transformation. In contrast to the Tsung group's strategy, the NP@Cu_2O core–shell nanostructures serve as a sacrificial core–shell template. The Cu^{2+} ions generated *via* the oxidative dissolution of the Cu_2O shell in the mildly acidic H_3BTC solution could be used as a metal ion source to grow Cu-BTC (HKUST-1) crystals. The NP@HKUST-1 heterosuperstructures exhibited a yolk–shell petalous morphology with a certain degree of mesoporosity. The morphology of the yolk–shell superstructures relied on the intricate balance between the dissolution rate of the Cu_2O and the crystal growth rate of the metal ions with the ligands, which was influenced by the concentration of the reactants, the reaction temperature, and the polarity of the solvent.

3.4.2. Sacrificial single-crystal template. In 2016, Lou *et al.* reported the preparation of hollow ZIF-67 prism-like nanostructures using cobalt acetate hydroxide nanoprisms as a sacrificial single-crystal template (Fig. 11).[20] After rapidly adding the Co precursors dispersed in ethanol into a 2-MeIM ethanol solution, refluxing the mixed solution at 110 °C produced the hollow ZIF-67 prism-like nanostructures. The evolution of the hollow interior was ascribed to the diffusion of the metal ions and organic ligands during the formation of the ZIF-8 superstructures. The outward diffusion of the small Co^{2+} ions from the prismatic surface of the single-crystalline precursors initiates the growth of ZIF-67 polyhedral nanoparticles over the sacrificial template to form hollow prismatic nanostructures with a well-defined internal void. The morphology and robustness of the hollow ZIF-67 nanostructures were significantly influenced by the concentration of the organic ligands and the solvent.

In 2015, Lah *et al.* reported the preparation of single-crystalline hollow MOF octahedral superstructures using MOP single crystals as a sacrificial template (Fig. 12).[21] The authors added air-dried Cu-MOP single crystals into a methanol solution containing ditopic linkers such as dabco, pyrazine (pz), and 4,4′-bipyridine (bpy). Hollow MOF single crystals precipitated out from this solution, wherein the Cu-MOPs were linked *via* the ditopic linkers to form 3-D MOF $[Cu_{24}(hip)_{24}L_6(H_2O)_{12}]$ (H_2hip = 5-hydroxyisophthalic acid; L = ditopic linker). The

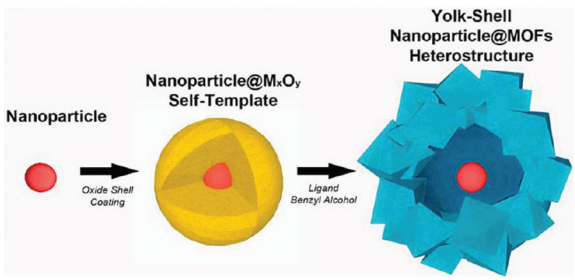

Fig. 10 Schematic illustration of a hollow Au@HKUST-1 superstructure using a Au@Cu_2O core–shell as a sacrificial core–shell template. Reprinted with permission from ref. 19. © 2013 American Chemical Society.

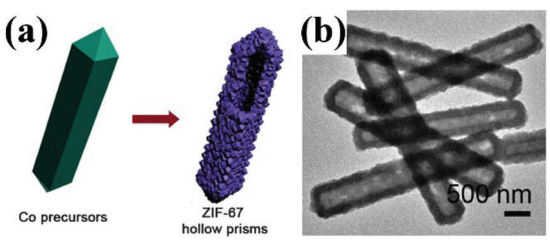

Fig. 11 (a) Schematic illustration of the formation of a hollow ZIF-67 prism using a cobalt acetate hydroxide nanoprism as a sacrificial single-crystal template and (b) a TEM image of hollow ZIF-67 prisms. Reproduced with permission from ref. 20. © 2016 Wiley-VCH.

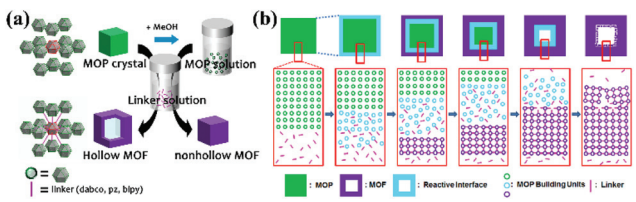

Fig. 12 (a) Schematic illustrations of (a) the formation of a single-crystalline hollow MOF using a MOP single crystal as a sacrificial template and (b) the proposed formation mechanism. Reprinted with permission from ref. 21. ©The Royal Society of Chemistry.

single-crystalline hollow MOF shells formed *via* outward diffusion of the Cu-MOP building blocks from the surface of the MOP crystal templates to the methanol solution containing the linkers. The formation of the hollow structure was dependent on the type and concentration of the linker and the solvent employed. The dimensions of the hollow structures could be controlled by the dimensions of the sacrificial MOP single crystals.

Furukawa and Kitagawa's research team demonstrated the preparation of hollow MOF box superstructures using MOF single crystals as a sacrificial template.[22] Heating the cuboidal MOF $[Zn_2(NDC)_2(bpy)]$ (NDC = 1,4-naphthalenedicarboxylate) parent crystals in the solution of H_2BDC led to the formation of hollow box superstructures made of two-fold interpenetrated solid-solution MOF $[Zn_2(BDC)_{1.5}(NDC)_{0.5}(bpy)]$ crystals. The reaction of BDC, which diffused inward from the bulk solution toward the surface of the parent MOF crystals, with Zn^{2+}, NDC and bpy components, which diffused outward from the parent MOF crystals, resulted in the recrystallization of the solid-solution MOF, which exhibited a hollow box superstructure morphology, wherein the parent MOF crystal simultaneously served as both a crystalline template and a reactant.

4. Soft template strategies

Although hard template strategies for hollow superstructures are simple and straightforward to apply, the strategies are limited to core–shell structures whose core and shell exhibit significantly different dissolution properties. However, etching the hard template often severely deteriorates the inherent properties of the shell of the hollow superstructures. In contrast, a soft template approach often allows the facile removal of the soft template from the core–shell structures. However, controlling the morphology of hollow superstructures using a soft template strategy is restrained to mainly a spherical shape due to the inherent difficulties in modulating the soft template into a shape other than a sphere.

4.1. Micelle template and cell wall template

4.1.1. Micelle template. Wang *et al.* reported the fabrication of surfactant-crosslinked PB nanoshells using an approach called miniemulsion periphery polymerization (MEPP).[23a] A micelle template containing pentacyanoferrate terminal groups was prepared in a mixed solvent consisting of toluene, hexadecane, and water using an organometallic surfactant, poly(ethylene glycol)-*b*-poly(propylene glycol)-*b*-poly(ethylene glycol) terminated with pentacyano(4-(dimethylamino)pyridine)ferrate (EPE-Fe). The addition of Fe^{3+} ions into the solution containing the micelles resulted in amorphous Fe-PB nanoshells polymerized at the periphery of the micelle template, and the micelle served as both a template and the source of the reactants, namely iron and cyanide ions, for the surfactant-crosslinked Fe-PB nanoshells. The same group reported surfactant-free hollow MFe-PB analogue superstructures (where, M = Gd, Er) by detaching the crosslinked-surfactant from the MFe-PB analogue nanoshells (Fig. 13).[23b] The MFe-PB analogue nanoshells were obtained by adding lanthanide ions such as Gd^{3+} and Er^{3+} instead of Fe^{3+} ions into the solution containing the micelles. Repeated cycles of shaking/stirring the MFe-PB analogue nanoshells in fresh MeOH and decanting the solvent produced surfactant-free hollow MFe-PB analogue superstructures.

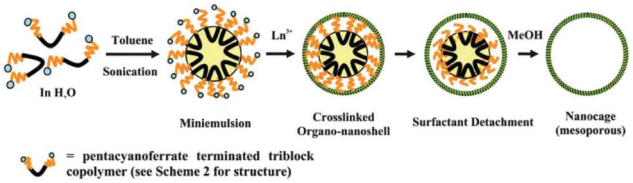

Fig. 13 Synthetic protocol towards surfactant-free hollow MFe-PB analogue superstructures. Reprinted with permission from ref. 23*b*. © 2011 The Royal Society of Chemistry.

Lei *et al.* prepared crystalline ZIF-8 hollow nanospheres using sodium dodecyl sulfate (SDS) as a micelle template.[23c] The ZIF-8 hollow nanospheres were prepared by the addition of Zn^{2+} ions and 2-MeIM into an SDS aqueous solution. The SDS surfactants in the ZIF-8 hollow nanospheres were removed simply by washing the product with deionized water and drying it in air under 100 °C.

4.1.2. Cell wall template. In 2016, Zhang *et al.* introduced cell walls from natural biomaterials as a hollow template to assemble MOF/cell wall (CW) microcapsules *via* inside/outside interfacial crystallization (IOIC) (Fig. 14).[24] To synthesize the hollow MOF/CW microcapsules, they prepared pure cell walls by washing the cells with methanol to remove the cytoplasm from the cells. After impregnating the cell walls with metal ions, the cell walls were dispersed in a linker solution, and the

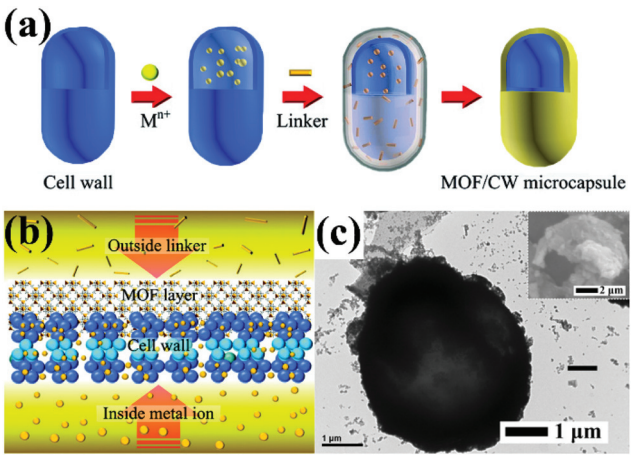

Fig. 14 Assembly of hollow MOF/CW microcapsules. (a) Synthetic method for the deposition of a MOF layer on a cell wall. (b) Crystallization of the MOF layer. (c) TEM image of a hollow ZIF-8/CW microcapsule. Reproduced with permission from ref. 24. © 2016 Wiley-VCH.

MOFs crystallized preferentially on the porous cell walls *via* a reaction between the separated metal ions inside the cell and the linkers on the outside of the cell. This strategy for fabricating MOF/CW microcapsules *via* IOIC was applied to various MOFs such as ZIF-8, HKUST-1, and MIL-53(Fe) and to the cell walls from both eukaryotic yeast cells and prokaryotic *Escherichia coli* cells. Though the cell wall templates were not removed, the MOF/CW superstructures were hollow structures since the cell walls themselves form a hollow structure. The assembled MOF/CW microcapsules exhibited good stability and the size-selective release of small molecules, and this size selectivity could be adjusted by changing the type of coated MOF.

4.2. Liquid template

4.2.1. *In situ* preparation of MOF nanoparticles using the reactants from two different liquid phases. De Vos *et al.* introduced the preparation of hollow MOF nanostructures *via* interfacial growth of a crystalline MOF layer using two immiscible flowing microfluidic liquids (Fig. 15a).[25a] Aqueous solution droplets containing metal ions were used as a spherical liquid template in a continuous organic solution containing linker ligands. Hollow capsules of HKUST-1 were prepared by injecting the aqueous phase containing Cu^{2+} ions with polyvinyl alcohol (PVA) as an emulsifier through a hollow needle in a co-flowing stream of the organic solution containing BTC ligand flowing through polytetrafluoroethylene tubing. The temporary spherical liquid template was removed during the simple washing process of the hollow capsules using ethanol with no additional etching process. The dimensions of the monodisperse hollow HKUST-1 capsules could be controlled by adjusting the ratio of the inner and outer flows.

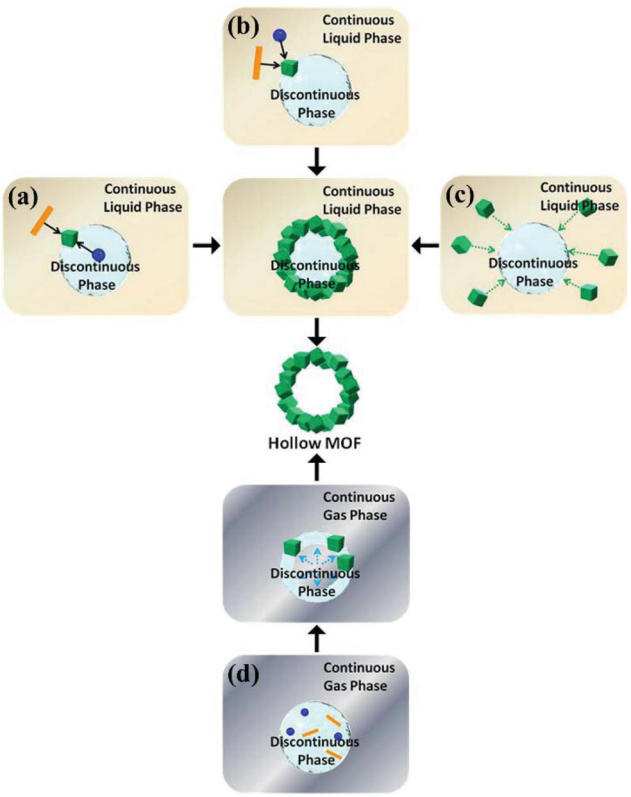

Fig. 15 Schematic illustration of the formation of hollow MOF superstructures. The hollow MOF superstructure was prepared *in situ* using reactants (a) from two different liquid phases and (b) from a continuous liquid phase. (c) Formation of a hollow MOF superstructure *via* the formation of a Pickering emulsion using pre-prepared MOF nanoparticles. (d) Spray drying strategy.

Falcaro and Kim's research team reported another hollow MOF superstructure *via* the same approach using MIL-88A.[25b] The architecture was extended to a double-shell hollow structure using double emulsion droplets generated from the serially coupled two pieces of T-junction microfluidic system. Moreover, various functional nanoparticles and enzymes were encapsulated in the hollow cavity while maintaining the functionality of the cargo.

Liu, Jiang and Xu's research team also reported an emulsion-based bidirectional interfacial reaction method to prepare hollow MOF superstructures.[25c] A water-in-oil nanoemulsion was first prepared with aqueous droplets containing Zn^{2+} ions using PVP as a stabilizer and 1-octanol as the continuous oil phase, and then, an organic solution containing 2-MeIM was added to the emulsion to initiate a bidirectional interfacial reaction between the aqueous droplet and the organic phase to grow ZIF-8 nanocrystals. The hollow ZIF-8 nanospheres could be obtained in large quantities with a high yield *via* this emulsion-based interfacial reaction method. The shell thickness of the hollow structure could be controlled by tuning the amount of precursors used or by varying the crystallization time. In addition, functional materials such as Pd nanocubes could be encapsulated in the hollow cavities by introducing the nanocubes during the emulsification process.

4.2.2. *In situ* preparation of MOF nanoparticles using the reactants from a single liquid phase. Eddaoudi *et al.* reported the synthesis and integration of MOF cubes into hollow microspheres using a single-step emulsion-based approach (Fig. 15b).[26] They prepared Fe-**soc**-MOF hollow microspheres by reacting Fe^{3+} as a metal ion and 3,3′,5,5′-azobenzenetetracarboxylic acid (H_4ABTC) as an organic ligand in a DMSO/CH_3CN/water mixed solvent in the presence of *tert*-butylamine (TBA) as a structure-directing agent (SDA) and polyoxyethylene sorbitan trioleate (Tween-85) as an emulsifying non-ionic surfactant. The monodisperse Fe-**soc**-MOF nanocubes prepared *in situ* aggregated to form hollow microspheres at the interface between the emulsion droplet and the continuous solution phase. The size of the hollow microsphere could be controlled by the amount of Tween-85. The diameter of the hollow microsphere decreased with the increasing concentration of Tween-85. Eddaoudi's group also reported isostructural hollow microspheres by integrating tetrakaidecahedral Ga-**soc**-MOF building blocks using a similar single-step emulsion-based approach.[13c] Triethylamine (TEA) was chosen as a SDA to regulate the crystal growth of the tetrakaidecahedral building blocks, and sorbitan trioleate (Span-85) was used as a surfactant with dioctyl sulfosuccinate sodium salt (AOT) as a co-surfactant to form emulsion droplets as soft liquid templates.

4.2.3. Pre-prepared MOF nanoparticles. Xiao *et al.* observed that pre-prepared MOF nanoparticles could be used to form a Pickering emulsion (Fig. 15c).[27a] An aqueous dispersion of HKUST-1 nanoparticles with no surface modifications could be used as an aqueous phase for the subsequent preparation of water–oil emulsions (note that the oil used in the experiment was not specified) with no additional surfactant, wherein the HKUST-1 nanoparticles at the oil/water interface stabilized both oil-in-water and water-in-oil emulsions. However, the evaporation of the aqueous phase from the oil-in-water emulsion did not lead to intact hollow HKUST-1 spherical superstructures since the interaction between HKUST-1 nanoparticles was not strong enough to maintain the form of the Pickering emulsion droplets.

Huo and Bradshaw's research team reported the preparation of polymer-reinforced MOF microcapsules derived from Pickering emulsions.[27b] Oily dodecane containing styrene and divinylbenzene together with azobisisobutyronitrile as an initiator, which is necessary for cross-linking the PS membrane, was added into an aqueous solution containing dispersed MOF nanoparticles such as ZIF-8, MIL-101, and Benz-UiO-66 particles. Then, the mixture was agitated to form a Pickering emulsion stabilized by the MOF nanoparticles. Subsequently heating the Pickering emulsion initiated the polymerization to form cross-linked PS membranes within the oil droplets and hollow MOF@PS microcapsules, in which microporous MOF nanoparticles were embedded within the surface of the polymer shell.

4.2.4. Pre-prepared MOF nanoparticles and the subsequent *in situ* preparation of MOF nanoparticles using the reactants from a single liquid phase. Huo and Bradshaw's research team also prepared MOF-reinforced hollow MOF-A@MOF-B microcapsules wherein a shell of MOF-A was stabilized with a hierarchical MOF-B capsule shell prepared *via* a two-step synthesis using Pickering emulsions.[28] An inverse phase Pickering emulsion stabilized with pre-hydrophobized Hep-UiO-66 and Hep-Fe_3O_4 nanoparticles was prepared, wherein agarose hydrogel droplets were dispersed in a continuous paraffin oil phase. The Pickering emulsion was immersed in a $Zn(NO_3)_2$ solution in isopropanol, followed by the addition of 2-MeIM in isopropanol. Maintaining the solution at low temperature led to the rapid precipitation of ZIF-8 particles to aggregate into a network, which provided additional stabilization to the Hep-UiO-66/Hep-Fe_3O_4 Pickering emulsion as the aggregation occurred around the Hep-UiO-66/Hep-Fe_3O_4 nanoparticles as the first step. Then, dense ZIF-8 shells were slowly grown in 2-butanol to yield robust hollow Hep-UiO-66/Hep-Fe_3O_4@ZIF-8 microcapsules. The thickness of the hierarchical ZIF-8 capsule shell could be controlled by the number of repeated growth cycles during this final growth step. In addition, functional biomolecules could be easily encapsulated in the hollow cavity of the microcapsules by the inclusion of the biomolecules within the Hep-UiO-66/Hep-Fe_3O_4 stabilized hydrogel droplets during the formation of the Pickering emulsion.

4.2.5. Spray drying. Spray drying is another strategy for the formation of hollow superstructures at the liquid–gas interface using liquid droplets as a soft template in a continuous gas phase. In 2013, Maspoch *et al.* adopted a spray-drying strategy to prepare hollow MOF superstructures (Fig. 15d).[29a] The spray drying strategy mimics the strategy employing emulsion droplets as a liquid template but does not require a secondary immiscible liquid solvent. The hollow MOF superstructures were obtained by spraying a solution of MOF precursors under co-flowing drying gas using a two-fluid nozzle into the drying chamber as fine liquid microdroplets. These microdroplets were then dried into solid hollow superstructures, and the solid product was collected in a glass collector under the cyclone. This methodology was applied to a series of representative MOFs such as HKUST-1, NOTT-100, MIL-88A, MIL-88B, MOF-14, MOF-74, and UiO-66.

Hollow ZIF-8 and Cu-PB superstructures were obtained using a slightly modified methodology, either using a three-fluid nozzle or a two-fluid nozzle. The three-fluid nozzle could simultaneously spray two separate solutions containing the metal ions and organic ligands under co-flowing drying gas. The two-fluid nozzle could spray a solution mixed in a connector inserted before the two-fluid nozzle under co-flowing drying gas. The size of the hollow MOF superstructures could be controlled by varying the precursor concentration, flow rate, and inlet temperature.

Marquez and Boissiere's research team independently reported the preparation of hollow MOF superstructures *via* the same spray drying strategy using a concentric three-fluid nozzle (*i.e.*, by mixing fluid 1, fluid 2, and air).[29b] Simultaneously injecting two separate solutions with the organic ligands and the metal salts, which can lead to HKUST-1 and MIL-100(Fe), respectively, into the same flow of hot air led to the corresponding poly-dispersed hollow MOF microspheres.

4.3. Gas template strategy

The gas template strategy is similar to the spray drying strategy in that the superstructures form at the liquid–gas interface. However, the spray drying strategy sprays liquid droplets into a drying gas as a soft liquid template, while the gas template strategy employs discontinuous gas bubbles in a continuous liquid phase as a soft gas template.

4.3.1. Gas template in an ionic liquid. In 2014, Zhang *et al.* demonstrated the preparation of hollow MOF microparticles using CO_2 bubbles as a gas template in ionic liquids (ILs).[30] Mixtures of hollow Zn-BTC spherical microcapsules and hollow Zn-BTC tetrahedron-like microparticles were obtained from 1,1,3,3-tetramethylguanidine trifluoroacetate (an IL) containing the MOF precursors, CO_2 bubbles and a surfactant. The morphologies of the hollow microparticles could be easily controlled by the CO_2 pressure and surfactant concentration. While agglomerates of Zn-BTC nanocrystals were obtained only in the absence of CO_2 bubbles, CO_2 bubbles at high pressure resulted in more micron-sized Zn-BTC tetrahedral capsules. Moreover, the reaction at a low surfactant concen-

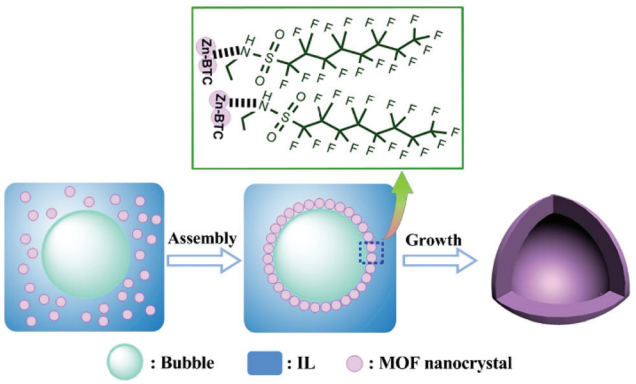

Fig. 16 Schematic illustration of the formation of a hollow Zn-BTC sphere *via* a CO_2–IL interfacial templating route and the subsequent surfactant-directed growth into a hollow Zn-BTC tetrahedron-like microparticle. Reprinted with permission from ref. 30. © 2013 Elsevier.

tration under a fixed CO_2 pressure led to hollow spherical microcapsules, while the same reaction at a higher surfactant concentration under the same CO_2 pressure yielded hollow tetrahedron-like microcapsules. The MOF nanocrystals formed at the CO_2–IL interface assembled into hollow spherical capsules, which subsequently converted into hollow tetrahedral capsules *via* anisotropic crystal growth directed by the surfactant (Fig. 16). When the experimental conditions were kept the same but the ligand was replaced by H_2BDC, hollow Zn-BDC polyhedral prismatic microcapsules were obtained. However, the correlation between the morphologies of the hollow capsules and the reaction conditions such as CO_2 pressure, surfactant concentration, and ligands employed were not well understood.

5. Summary and outlook

Since the first report on a microporous hollow coordination polymer superstructure by Wang and his co-workers in 2010,[10a] more than 80 hollow MOF superstructures have been reported using strategies similar to those for the fabrication of hollow M/MO nano/microstructures. In this review, the strategies for hollow MOF superstructures have been classified by the use of external templates and by the types and properties of these templates.

Many hollow MOF superstructures have been obtained without external templates. Intermediates obtained as an unstable species during reactions convert to the final hollow MOF superstructures either *via* dissolution of the core region of the intermediate and recrystallization at the shell region of the intermediate by the Ostwald ripening mechanism or *via* mass transfer from the unstable concave surface of the intermediate to the stable surface of the hollow shell, which is driven by the surface energy. In the self-template mechanism, the kinetic intermediate obtained as an unstable species during the reaction simultaneously serves as both a hard template and a sacrificial template. Surface-protected selective etching is also a template-free strategy, but it is different from the other template-free strategies. The surface-protected selective etching is a top-down approach for hollow structures, where the hollow cavity is generated *via* selective etching of the core region of the surface-protected single crystals. However, hollow MOF superstructures from the other template-free strategies are obtained *via* bottom-up approaches. The hollow cavities are generated *via* the self-assembly of the MOF shells.

Most hollow MOF superstructures were obtained using external templates. After the core–shell core@MOF structure is prepared using an external template, the core of the core–shell structure is selectively etched to generate a hollow MOF superstructure. When the template is a hard template, the formation of core–shell structures and the proper etching process are critical processes for successfully obtaining hollow MOF structures. In the case of an amorphous solid template, forming a hollow structure with a non-spherical shape is not easy due to the inherent difficulty in controlling the shape of an amorphous solid particle. The morphologies of hollow MOF superstructures can be better controlled using a crystalline solid template with a well-defined morphology; however, preparing a core–shell structure is often limited to an isostructural core/shell pair. Hollow superstructures can be obtained *via* either a stepwise or one-step process. While the core region of the core–shell structure precursor is selectively etched in the stepwise approach, the formation of the shell occurs simultaneously together with the dissolution of the core in the one-step process. Hollow MOF superstructures can also be obtained using a sacrificial hard template with no additional etching process wherein the template is consumed as a reactant.

Soft templates such as liquid droplets and gas bubbles can also be employed to prepare hollow MOF superstructures. Hollow MOF shells can be self-assembled *in situ* at the interface between discontinuous spherical liquid droplets or gas bubbles and another continuous fluid phase. In these approaches, the building blocks of the MOF shell can be supplied all together in a single phase (either the discontinuous or continuous phase) or separately in two different phases. Hollow MOF superstructures can also be generated *via* the aggregation of pre-prepared MOF nanocrystals at the interface of a Pickering emulsion. While template removal is more facile with a soft template than with a hard template, controlling the morphology of the hollow superstructure is expected to be more difficult. However, there has been a report on hollow superstructures with tetrahedron-like and polyhedral-prism-like morphologies using CO_2 bubbles as a soft gas template in an IL.[26] The surfactant was proposed as a directing agent for the anisotropic growth of the MOF crystals, though the details of the mechanism were not provided.

MOF superstructures have exhibited collective and/or synergistic effects in applications such as catalysis,[11a,b,16c,18,19,25b,c,28,30] separation,[22,25a,31] storage,[13b] sensors,[32] reactors,[33] photoluminescence,[10b] anodes for lithium-ion batteries,[34a,b] and precursors for other hollow nanostructures.[10d,16b,20] Further progress in the development of fabrication strategies

for hollow MOF superstructures, including controlling the size and morphology of the superstructures, could ultimately lead to practical applications of the materials in various areas.

Acknowledgements

This work was supported by the National Research Foundation of Korea (2015R1A2A1A15053104, 2015R1D1A1A01056579, and 2016R1A5A1009405).

References

1 (*a*) H.-C. Zhou and S. Kitagawa, *Chem. Soc. Rev.*, 2014, **43**, 5415–5418; (*b*) H. Furukawa, K. E. Cordova, M. O'Keeffe and O. M. Yaghi, *Science*, 2013, **341**, 1230444; (*c*) H.-C. Zhou, J. R. Long and O. M. Yaghi, *Chem. Rev.*, 2012, **112**, 673–674; (*d*) J. R. Long and O. M. Yaghi, *Chem. Soc. Rev.*, 2009, **38**, 1213–1214.

2 (*a*) G. M. Whitesides and M. Boncheva, *Proc. Natl. Acad. Sci. U. S. A.*, 2002, **99**, 4769–4774; (*b*) H. Cölfen and S. Mann, *Angew. Chem., Int. Ed.*, 2003, **42**, 2350–2365; (*c*) M. Boncheva and G. M. Whitesides, *MRS Bull.*, 2005, **30**, 736–742; (*d*) Y. Min, M. Akbulut, K. Kristiansen, Y. Golan and J. Israelachvili, *Nat. Mater.*, 2008, **7**, 527–538; (*e*) Z. Nie, A. Petukhova and E. Kumacheva, *Nat. Nanotechnol.*, 2010, **5**, 15–25.

3 (*a*) A. Carné-Sánchez, I. Imaz, K. C. Stylianou and D. Maspoch, *Chem. – Eur. J.*, 2014, **20**, 5192–5201; (*b*) S. Furukawa, J. Reboul, S. Diring, K. Sumida and S. Kitagawa, *Chem. Soc. Rev.*, 2014, **43**, 5700–5734; (*c*) B. Seoane, S. Castellanos, A. Dikhtiarenko, F. Kapteijn and J. Gascon, *Coord. Chem. Rev.*, 2016, **307**, 147–187.

4 (*a*) H. C. Zeng, *J. Mater. Chem.*, 2006, **16**, 649–662; (*b*) X. W. Lou, L. A. Archer and Z. Yang, *Adv. Mater.*, 2008, **20**, 3987–4019; (*c*) H. C. Zeng, *J. Mater. Chem.*, 2011, **21**, 7511–7526.

5 H. G. Yang and H. C. Zeng, *J. Phys. Chem. B*, 2004, **108**, 3492–3495.

6 F. Caruso, R. A. Caruso and H. Möhwald, *Science*, 1998, **282**, 1111–1114.

7 H. Cao, X. Qian, C. Wang, X. Ma, J. Yin and Z. Zhu, *J. Am. Chem. Soc.*, 2005, **127**, 16024–16025.

8 (*a*) A. D. Smigelskas and E. O. Kirkendall, *Trans. AIME*, 1947, **171**, 130–142; (*b*) W. Wang, M. Dahl and Y. Yin, *Chem. Mater.*, 2013, **25**, 1179–1189; (*c*) Y. Yin, R. M. Rioux, C. K. Erdonmez, S. Hughes, G. A. Somorjai and A. P. Alivisatos, *Science*, 2004, **304**, 711–714.

9 (*a*) A. M. Collins, C. Spickermann and S. Mann, *J. Mater. Chem.*, 2003, **13**, 1112–1114; (*b*) H. G. Yang and H. C. Zeng, *Angew. Chem., Int. Ed.*, 2004, **43**, 5206–5209.

10 (*a*) J. Huo, L. Wang, E. Irran, H. Yu, J. Gao, D. Fan, B. Li, J. Wang, W. Ding, A. M. Amin, C. Li and L. Ma, *Angew. Chem., Int. Ed.*, 2010, **49**, 9237–9241; (*b*) S.-L. Zhong, R. Xu, L.-F. Zhang, W.-G. Qu, G.-Q. Gao, X.-L. Wu and A.-W. Xu, *J. Mater. Chem.*, 2011, **21**, 16574–16580; (*c*) J. Huo, L. Wang, E. Irran, H. Yu, L. Ma, J. Gao, D. Fan, W. Ding, A. M. Amin and Y. Tai, *J. Colloid Interface Sci.*, 2012, **367**, 92–100; (*d*) Z. Shen, J. Liu, F. Hu, S. Liu, N. Cao, Y. Sui, Q. Zeng and Y. Shen, *CrystEngComm*, 2014, **16**, 3387–3394.

11 (*a*) Z. Zhang, Y. Chen, X. Xu, J. Zhang, G. Xiang, W. He and X. Wang, *Angew. Chem., Int. Ed.*, 2014, **53**, 429–433; (*b*) Z. Zhang, Y. Chen, S. He, J. Zhang, X. Xu, Y. Yang, F. Nosheen, F. Saleem, W. He and X. Wang, *Angew. Chem., Int. Ed.*, 2014, **53**, 12517–12521.

12 I. Lee, S. Choi, H. J. Lee and M. Oh, *Cryst. Growth Des.*, 2015, **15**, 5169–5173.

13 (*a*) M. Hu, S. Furukawa, R. Ohtani, H. Sukegawa, Y. Nemoto, J. Reboul, S. Kitagawa and Y. Yamauchi, *Angew. Chem., Int. Ed.*, 2012, **51**, 984–988; (*b*) M. Hu, N. L. Torad and Y. Yamauchi, *Eur. J. Inorg. Chem.*, 2012, **30**, 4795–4799; (*c*) X. Cai, X. Deng, Z. Xie, S. Bao, Y. Shi, J. Lin, M. Pang and M. Eddaoudi, *Chem. Commun.*, 2016, **52**, 9901–9904; (*d*) M. Hu, Y. Ju, K. Liang, T. Suma, J. Cui and F. Caruso, *Adv. Funct. Mater.*, 2016, **26**, 5827–5834.

14 J. Lee, J. H. Kwak and W. Choe, *Nat. Commun.*, 2017, **8**, 14070.

15 (*a*) H. J. Lee, W. Cho and M. Oh, *Chem. Commun.*, 2012, **48**, 221–223; (*b*) A.-L. Li, F. Ke, L.-G. Qiu, X. Jiang, Y.-M. Wang and X.-Y. Tian, *CrystEngComm*, 2013, **15**, 3554–3559.

16 (*a*) O. N. Risset, E. S. Knowles, S. Ma, M. W. Meisel and D. R. Talham, *Chem. Mater.*, 2013, **25**, 42–47; (*b*) D. Cai, B. Liu, D. Wang, L. Wang, Y. Liu, B. Qu, X. Duan, Q. Li and T. Wang, *J. Mater. Chem. A*, 2016, **4**, 183–192; (*c*) J. Yang, F. Zhang, H. Lu, X. Hong, H. Jiang, Y. Wu and Y. Li, *Angew. Chem., Int. Ed.*, 2015, **54**, 10889–10893; (*d*) C. Rösler, A. Aijaz, S. Turner, M. Filippousi, A. Shahabi, W. Xia, G. Van Tendeloo, M. Muhler and R. A. Fischer, *Chem. – Eur. J.*, 2016, **22**, 3304–3311.

17 L.-Y. Chou, P. Hu, J. Zhuang, J. V. Morabito, K. C. Ng, Y.-C. Kao, S.-C. Wang, F.-K. Shieh, C.-H. Kuo and C.-K. Tsung, *Nanoscale*, 2015, **7**, 19408–19412.

18 C.-H. Kuo, Y. Tang, L.-Y. Chou, B. T. Sneed, C. N. Brodsky, Z. Zhao and C.-K. Tsung, *J. Am. Chem. Soc.*, 2012, **134**, 14345–14348.

19 Y. Liu, W. Zhang, S. Li, C. Cui, J. Wu, H. Chen and F. Huo, *Chem. Mater.*, 2014, **26**, 1119–1125.

20 L. Yu, J. F. Yang and X. W. Lou, *Angew. Chem., Int. Ed.*, 2016, **55**, 13422–13426.

21 H. Kim, M. Oh, D. Kim, J. Park, J. Seong, S. K. Kwak and M. S. Lah, *Chem. Commun.*, 2015, **51**, 3678–3681.

22 K. Hirai, J. Reboul, N. Morone, J. E. Heuser, S. Furukawa and S. Kitagawa, *J. Am. Chem. Soc.*, 2014, **136**, 14966–14973.

23 (*a*) G. Liang, J. Xu and X. Wang, *J. Am. Chem. Soc.*, 2009, **131**, 5378–5379; (*b*) R. McHale, Y. Liu, N. Ghasdian, N. S. Hondow, S. Ye, Y. Lu, R. Brydson and X. Wang, *Nanoscale*, 2011, **3**, 3685–3694; (*c*) X. Cao, L. Dai, L. Wang, J. Liu and J. Lei, *Mater. Lett.*, 2015, **161**, 682–685.

24 W. Li, Y. Zhang, Z. Xu, Q. Meng, Z. Fan, S. Ye and G. Zhang, *Angew. Chem., Int. Ed.*, 2016, **55**, 955–959.

25 (*a*) R. Ameloot, F. Vermoortele, W. Vanhove, M. B. J. Roeffaers, B. F. Sels and D. E. De Vos, *Nat. Chem.*, 2011, **3**, 382–387; (*b*) G.-Y. Jeong, R. Ricco, K. Liang, J. Ludwig, J.-O. Kim, P. Falcaro and D.-P. Kim, *Chem. Mater.*, 2015, **27**, 7903–7909; (*c*) Y. Yang, F. Wang, Q. Yang, Y. Hu, H. Yan, Y.-Z. Chen, H. Liu, G. Zhang, J. Lu, H.-L. Jiang and H. Xu, *ACS Appl. Mater. Interfaces*, 2014, **6**, 18163–18171.

26 M. Pang, A. J. Cairns, Y. Liu, Y. Belmabkhout, H. C. Zeng and M. Eddaoudi, *J. Am. Chem. Soc.*, 2013, **135**, 10234–10237.

27 (*a*) B. Xiao, Q. Yuan and R. A. Williams, *Chem. Commun.*, 2013, **49**, 8208–8210; (*b*) J. Huo, M. Marcello, A. Garai and D. Bradshaw, *Adv. Mater.*, 2013, **25**, 2717–2722.

28 J. Huo, J. Aguilera-Sigalat, S. El-Hankari and D. Bradshaw, *Chem. Sci.*, 2015, **6**, 1938–1943.

29 (*a*) A. Carné-Sánchez, I. Imaz, M. Cano-Sarabia and D. Maspoch, *Nat. Chem.*, 2013, **5**, 203–211; (*b*) A. G. Marquez, P. Horcajada, D. Grosso, G. Ferey, C. Serre, C. Sanchez and C. Boissiere, *Chem. Commun.*, 2013, **49**, 3848–3850.

30 L. Peng, J. Zhang, J. Li, B. Han, Z. Xue, B. Zhang, J. Shi and G. Yang, *J. Colloid Interface Sci.*, 2014, **416**, 198–204.

31 S. Hwang, W. S. Chi, S. J. Lee, S. H. Im, J. H. Kim and J. Kim, *J. Membr. Sci.*, 2015, **480**, 11–19.

32 N. Shi, Y. Zhang, D. Xu, C. Song, X. Jin, D. Liu, L. Xie and W. Huang, *New J. Chem.*, 2015, **39**, 9275–9280.

33 F. Zhang, Y. Wei, X. Wu, H. Jiang, W. Wang and H. Li, *J. Am. Chem. Soc.*, 2014, **136**, 13963–13966.

34 (*a*) H. Fei, X. Liu and Z. Li, *Chem. Eng. J.*, 2015, **281**, 453–458; (*b*) C. Li, X. Lou, M. Shen, X. Hu, Z. Guo, Y. Wang, B. Hu and Q. Chen, *ACS Appl. Mater. Interfaces*, 2016, **8**, 15352–15360.